*Archives Italiennes de Biologie, 145: 311-323, 2007.*

# POSTNATAL ELECTRICAL AND MORPHOLOGICAL ABNORMALITIES IN LUMBAR MOTONEURONS FROM TRANSGENIC MOUSE MODELS OF AMYOTROPHIC LATERAL SCLEROSIS

J. AMENDOLA, J.P. GUERITAUD, B. LAMOTTE D'INCAMPS [1], C. BORIES, S. LIABEUF, C. ALLENE, A. PAMBO-PAMBO, AND J. DURAND

*Laboratoire de Plasticité et Physio-Pathologie de la Motricité, UMR 6196 CNRS, Aix-Marseille Université, 31 Chemin Joseph Aiguier, 13402 Marseille cedex 20, France, 1 Laboratoire de Neurophysique et Physiologie, UMR 8119, CNRS,Université René Descartes, Paris, France*

## INTRODUCTION

Amyotrophic lateral sclerosis (ALS) is a human neurodegenerative disease characterized by a selective loss of motor neurons in spinal cord, brainstem and motor cortex. Mutation of Cu/Zn-superoxide dismutase (SOD1) is one proven cause of familial ALS (25). Although more than 110 mutations in the SOD1 gene are known to be responsible for ALS, only a subset of familial ALS cases is related to dominant missense mutations of SOD1 gene. However, sporadic and familial forms of the disease are clinically indistinguishable suggesting that they may share common mechanisms (7, 9). The initial mechanisms underlying the progressive degeneration of motoneurons and the disconnection between motor axons and muscular fibres can be studied in transgenic mouse models of ALS (7, 9, 12). We have detected early abnormalities during the maturation of motor systems in the $SOD1^{G85R}$ transgenic mouse model (1, 11). Further, we have recently shown that the mean input resistance of motoneurons from $SOD1^{G85R}$ mice was lower than that of wild type animals whereas their membrane capacitance was increased, suggesting a larger size of $SOD1^{G85R}$ motoneurons (3). In the present work, we tested this hypothesis using intracellular staining. On the other hand, the gain of lumbar motoneurons from $SOD1^{G85R}$ mouse pups was found to be lower than that of WT pups (3). It has been well established that activation of persistent inwards currents influence the gain of motoneurons (13, 19). Furthermore, an intrinsic hyperexcitability of mutant spinal motoneurons has been described in culture and organotypic slice culture derived from embryonic or neonate $SOD1^{G93A}$ mice (17, 18, 23). An increased persistent sodium inward current was involved in this hyperexcitability (18). Thus, we are studying the repetitive firing of the developing motoneurons and we report the effects of Riluzole, a blocker of persistent inward sodium current (26), on the discharge properties of motoneurons from $SOD1^{G85R}$ and $SOD1^{G93A}$ mice.

Corresponding Author: J. Durand same address Tel.: 33 4 9116 4650; fax 33 4 9177 5084
E mail: durand@dpm.cnrs-mrs.fr

## METHODS

All surgical and experimental procedures were in conformity with the European Communities council directive (86/609/EEC). Some of the experimental procedures were described previously (1, 3). The SOD1$^{G85R}$, line 148 (6, 7, 27), SOD1$^{G93A}$ -low expressor line (10), Hb9-eGFP (14) and double SOD1$^{G93A}$/Hb9-eGFP transgenic mice were generously provided by U382 INSERM-Marseille. The same length of gestation was observed for wild type and transgenic mice. Postnatal day 0 (P0) was defined as the first 24 hrs after birth.

*Isolated brainstem spinal cord preparation of neonate mice*

Briefly, pups at postnatal days (P3-P10) were anesthetized by hypothermia. They were then decerebrated at a post-collicular level, eviscerated and pinned down onto a Petri dish. Dorsal craniotomy and laminectomy were performed, allowing the spinal cord and brainstem to be removed, placed in a recording chamber, and perfused with an artificial cerebrospinal fluid (ACSF) containing in mM: NaCl, 130; KCl, 4; MgCl2, 1.2; CaCl2, 4; NaH2PO4, 1; NaHCO3, 25; glucose, 30; oxygenated with a 95% O2-5% CO2 mixture, adjusted to pH 7.4. The temperature of bath solution was kept at 24°C by a servo-controller (Harvard TC-202A).

*Slice preparation*

Following the isolation of the spinal cord in the dissecting artificial cerebrospinal fluid as described above, the lumbar enlargement was then isolated and placed in a block of agar (2%) and mounted in a vibrating microtome (Leica 1000 VT). Slices (350-400 µm thick) were cut and placed in a recovery ACSF for 30 min. Individual slices were then transferred to a recording chamber, continuously perfused with recording ACSF. Motoneurons were visualized using infrared differential interference contrast microscopy with an Olympus BX51 upright microscope and a Hamamatsu camera. In the case of double transgenic SOD1$^{G93A}$/Hb9-eGFP mice, motoneurons were identified with GFP epifluorescence.

*Electrophysiology*

In the entire isolated spinal cord preparation, micropipettes for intracellular recording were filled with potassium acetate 2M and their resistances ranged between 80 and 130 Mohms.

The motoneurons were identified by their antidromic action potential evoked following the electrical stimulation of the cut ventral root L5. The fifth lumbar root has been chosen because it concerns fewer pools (thus less heterogeneous populations) compared to L1-L4 lumbar roots in the mouse (21). Motoneurons were impaled using the same angle and depth of penetrations (150-450 µm) from the ventral cord surface corresponding to the caudal part of the fifth lumbar segment. Thus, motoneuronal pools of the intrinsic musculature of the foot were particularly targeted (21). However, the nature (extensor or flexor) of the innervated muscles could not be determined in our experiments. Intracellular potentials were amplified with an Axoclamp-2B in current clamp (Bridge or DCC modes) and digitized at 10 kHz by A/D converter. The discharge of motoneurons was studied using current ramp protocols (slope: 0.22 – 1.47 nA/s; duration: 5.4 – 10.8 s).

In slice preparation, whole cell patch-clamp recordings were made from GFP positive motoneurons or presumed motoneurons (large cells in the ventro-lateral region of spinal cord) or. Patch electrodes (resistance 5-6 MΩ) were pulled on a Sutter P97 puller (Sutter Instrument company, CA, USA). Signals recorded using whole cell patch-clamp techniques were amplified and filtered using an Axoclamp 2B (Axon Instruments, CA, USA). Amplified signals were acquired at 10 kHz using a digidata 1322A converter and pClamp softwares (Axon Instruments).

*Morphology*

Motoneurons intracellularly recorded in the entire brainstem/spinal cord preparation were stained using electrodes filled with 2M-K-acetate and 4% neurobiotin. One to two hours after labelling of the motoneuron, the spinal cord was immersed in fixative (4% paraformaldehyde) overnight at 4°C and the blocks were then rinced with PBS (pH 7.4). Each block was placed on a

sliding microtome and cut in the transversal plane at 75µm thickness. Sections were mounted on slides and air-dried overnight. Neurobiotin was visualized using a standard avidin-HRP-diaminobenzidine staining procedure. Labelled motoneurons were reconstructed from serial sections (75 µm thick) first on a microscope equipped with camera lucida attachment and then on a microscope equipped with a computer interfaced motorized stage and z-axis optical encoder using Neurolucida software. The boundaries of transversal spinal cord sections were also traced as illustrated in Fig. 2.

For statistical analysis, non-parametric exact tests (permutation with general scores test) or the non parametric Mann-Whitney U test were used (StatXact 7.0 software). Unless otherwise stated, the results are expressed as mean ± sd.

## RESULTS

*Morphology of mutant motoneurons*

Intracellular labelling with neurobiotin were obtained from antidromically identified lumbar motoneurons (n=17) on *in vitro* neonatal entire brainstem/spinal cord preparation. Each motoneuron was characterized by its electrical and morphological properties (figg. 1A-1$E_2$). The large motoneurons were targeted since motoneurons with low input resistances (< 15 MΩ) were preferentially impaired in the transgenic animals (3) and that fast-fatigable motoneurons are first affected in both $SOD1^{G85R}$ and $SOD1^{G93A}$ mice (24).

The position and dendritic extension of labelled motoneurons relative to the ventral horn in the transversal plane was thus precisely determined as illustrated in figure 1$E_2$. The labelled motoneurons were located within the same ventro-lateral region and directions of the dendrites depend on the precise location of the cell bodies. The dendrites mainly projected in three directions (dorsal, dorso-lateral and median) when the soma was in close proximity to the ventral horn boundary (Figg. 2A and 2C) whereas dendrites also extend ventrally when the soma was located in a central location within the pool (Figs. 2B and 2D).

In the transversal plane, the dendritic arborizations extended up to the ventro-lateral borders of the cord; some dendritic terminations were found near the middle line and others in a distant dorsal region of the spinal cord. In the rostro-caudal plane, the labelled motoneurons were reconstructed from six to ten sections corresponding to a rostrocaudal extension of 450 to 750 µm.

The soma size, number and diameter of primary dendrites were comparable in WT (n=9) and $SOD1^{G85R}$ (n=8) motoneurons. For the WT motoneurons, the soma diameter (30.6 ± 3.5 $\mu$m), soma area (742 ± 178 $\mu m^2$), the estimated membrane surface area ($P.D^2$=2967 ± 711 $\mu m^2$), the number of primary dendrites (7,33 ± 1.32) and their mean diameter (4.99 ± 1.17 $\mu$m) were similar to those already published for developing lumbar motoneurons in mice (20). These values were not significantly different from those obtained from $SOD1^{G85R}$ motoneurons: soma diameter (28.84 ± 6.51 $\mu$m), soma area (682 ± 305 $\mu m^2$), estimated membrane surface area ($P.D^2$= 2729 ± 1221 $\mu m^2$), number of primary dendrites (7.13 ± 1.45) and mean diameter of stem dendrites (5 ± 1.1 µm).

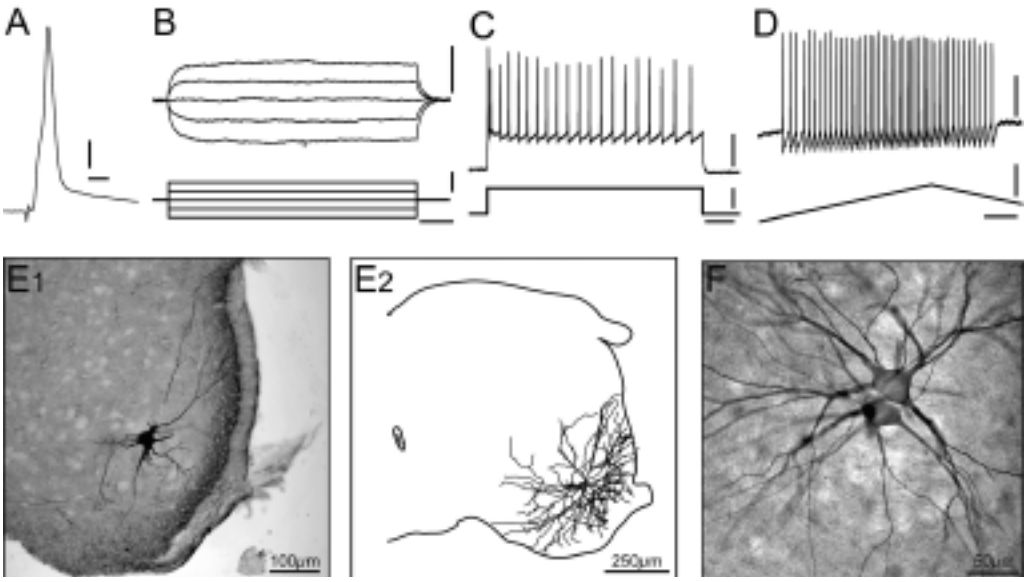


Fig. 1. - *Electrical and morphological characterization of identified lumbar motoneurons recorded from postnatal mice.*
A-E, all the data were obtained from the same motoneuron recorded from a P9 WT mouse.
A: Antidromic action potential (AP) elicited by the ventral root stimulation of the fifth lumbar segment (L5). Scale bars 1ms and 10mV. Resting membrane potential, Vm= -65mV.
B: Voltage deflections (top traces) recorded in response to a 350 ms test-pulse (-0.4 to 0.4 nA). No sag was observed in this range of current intensity. Only five traces derived from current steps of 0.05nA are illustrated. For this motoneuron, $R_{in}$ was of 10.7 MΩ. Scale bars 5mV, 0.4nA and 50ms.
C: Firing pattern obtained in response to long lasting (800ms) pulse of current (2.4 nA). The gain of this motoneuron was of 13.3 $Hz.nA^{-1}$ and the maximum firing frequency was 38.8 Hz. Scale bars 20mV, 2nA and 100ms.
D: Firing pattern elicited by triangular ramp stimulation. Note the firing rate adaptation on the descending phase indicating a clock-wise hysteresis (see fig. 4A). Scale bars 20mV, 1nA and 250ms.
$E_1$: Digital image from a transverse section of 75µm thick containing the soma filled with neurobiotin after electrophysiological recordings. Motor axon is not visible within this focal plane.
$E_2$: Transversal view of the digitized reconstruction of the same motoneuron showing the dendritic trees. Note the ventro-lateral location of the motoneuron also illustrated at a larger scale in fig. 2B.
F: Example of motoneurons coupled by gap junction and shown in a transverse section obtained from P8 $SOD1^{G85R}$ mouse. In some cases, a single intracellular injection of neurobiotin gave rise to several stained motoneurons precluding the 3D reconstruction. For these cells only the soma and primary dendrite diameters were obtained. Obj: 20x. Numerical zoom: 2x.

The total number of fully reconstructed cells (n=9 out of 17) was limited due to multiple staining indicating the presence of gap junctions (see Fig. 1F). The maximum difference of input resistances between WT and $SOD1^{G85R}$ motoneurons was found during P8-P9 period (3). We thus focused on the comparison of morphological properties during this period. At postnatal days 8-9 (P8-P9), full reconstructions using neurolucida were made in four cases (2 WT and 2 $SOD1^{G85R}$, see Fig. 2). These motoneurons have a comparable number of primary dendrites (n=8 in the two $SOD1^{G85R}$ motoneurons, n=7 and n=9 for the WT cases), similar mean diameters of primary dendrites and same dendritic projections according to the position of the

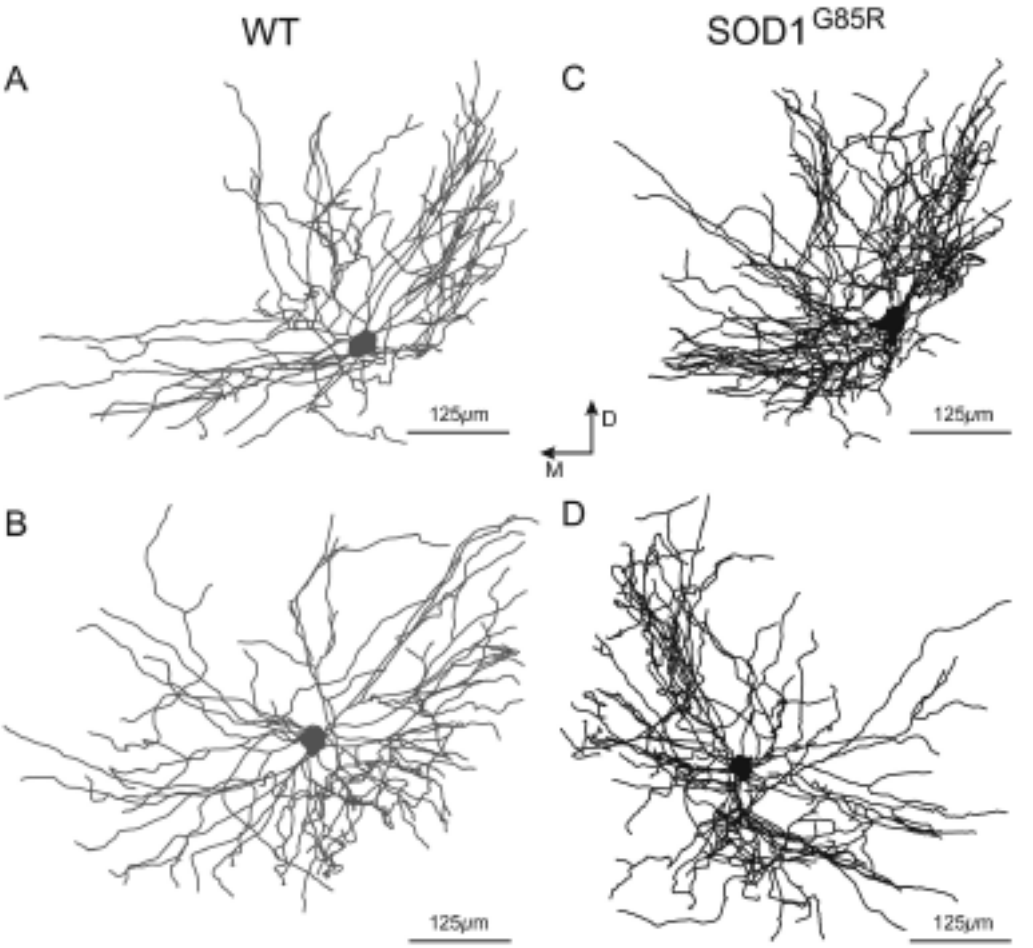


Fig. 2. - *Morphological differences between lumbar motoneurons from WT and SOD1$^{G85R}$ mice.*
A, B, C and D are two-dimensionnal projections of 4 digitized and fully reconstructed motoneurons. All the motoneurons were localized in the lateral part of the ventral horn (see fig. 1F). Same scale bars for all motoneurons, 125 $\mu$m.
A, B: Motoneurons obtained from WT mice (P9 and P8, respectively for A and B). Total dendritic length: 16771 $\mu$m and 13762 $\mu$m. Total dendritic membrane surface: 39978 $\mu m^2$ and 32653 $\mu m^2$. Numbers of branching points: 83 and 92. Numbers of terminals: 93 and 103 respectively for A and B.
C, D: Motoneurons obtained from SOD1$^{G85R}$ mice (P8 and P9, respectively for C and D). Total dendritic length: 20682 $\mu$m and 25262 $\mu$m. Total dendritic membrane surface: 39593 $\mu m^2$ and 46589 $\mu m^2$. Numbers of branching points: 147 and 154. Numbers of terminals: 162 and 172 respectively for C and D.
Note that for comparable morphology in term of dendrites directions and projections (A vs C, and B vs D), metric and topologic parameters were higher in SOD1$^{G85R}$ motoneurons.

soma in the nucleus. The longest dendritic path from soma to termination was similar in SOD1$^{G85R}$ (653 ± 52 $\mu$m) and WT motoneurons (649 ± 116 $\mu$m). However differences were found between WT and SOD1$^{G85R}$ dendritic trees for most others metric and topologic parameters (Table 1).

Table 1. - *Comparison of morphometric parameters in P8-9 motoneurons*

| | Total Dendritic Path length | Total Dendritic membrane Surface | Total branching points | Total terminations | Maximum branch order |
|---|---|---|---|---|---|
| **WT** | 15267 ± 2128 $\mu$m | 36316 ± 5180 $\mu m^2$ | 88 ± 6 | 98 ± 7 | 9 ± 1 |
| **SOD1$^{G85R}$** | 22972 ± 3239 µm | 43091 ± 4947 $\mu m^2$ | 151 ± 5 | 167 ± 7 | 15 ± 4 |

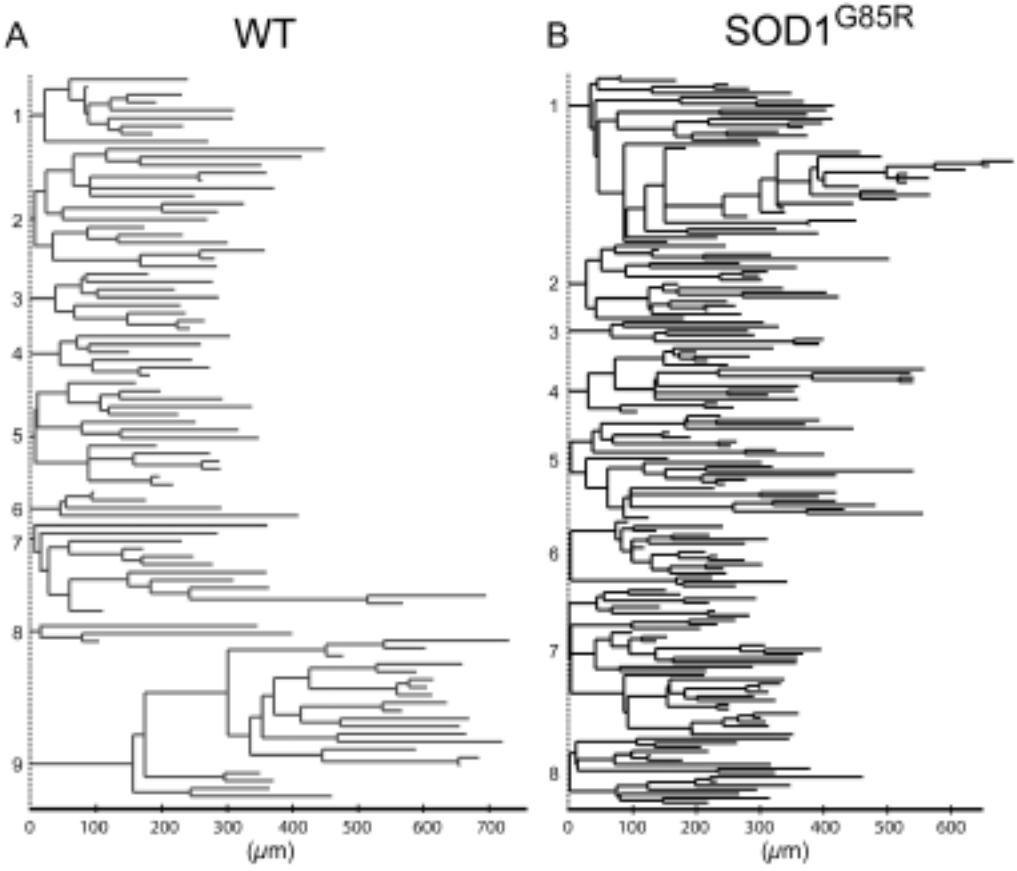


Fig. 3. - *Dendrites from SOD1$^{G85R}$ lumbar motoneurons were more develop and more complex compared to WT during the P8-P9 period.*
These dendrograms (bidimensionnal schematic representation) reveals that the dendrites are more complex in SOD1$^{G85R}$ motoneuron than in WT. Each dendrite was plotted as a function of the distance from the soma (in µm).
A, B: Dendrograms of the motoneurons shown in figure 2A and 2C. Note that for the WT motoneuron the mean length of dendritic trees was lower compared to SOD1$^{G85R}$ motoneurons as well as the number of branching nodes and terminals. Note that the number of primary dendrites was comparable (n=9 and n=8) as well as the maximal extension of the longest dendrites.

A highly complex morphology of dendrites was found in SOD1$^{G85R}$ compared to the WT motoneurons as shown in Figs. 2 and 3. Dendrograms in Fig. 3 A, B illustrate examples to emphasize the differences in the complexities of dendritic trees between WT and SOD1$^{G85R}$ motoneurons. Thus, the morphology of motoneurons from SOD1$^{G85R}$ mice displays important modifications at the postnatal period when we have found differences in input resistances (3).

*Electrical properties of postnatal motoneurons during ramp current injection*

Another difference in electrical properties concerned the lower gain of SOD1$^{G85R}$ motoneurons (3). In this set of experiments, we compared the electrical properties of WT and SOD1$^{G85R}$ motoneurons during ramp current injection.

Four different patterns of discharge were recorded in response to current ramp stimulation both for WT (n=19) and SOD1$^{G85R}$ (n=19) motoneurons. Since developmental changes are likely to occur during the time period we investigated (P3-P10), recordings were obtained from WT and SOD1$^{G85R}$ mice from similar numbers of motoneurons at the different ages, P3-P6: n=12 (WT) and n=10 (SOD1); P7-P10: n=7 (WT) and n=9 (SOD1). Figure 4 illustrates the different types of discharge that were recorded (left), with their corresponding F-I curves plotted for the depolarizing (filled triangles; up) and repolarizing (empty triangles, down) phases of the ramp. A clockwise hysteresis as shown by F-I curve (Fig. 4A) was observed in 8 WT and 5 SOD1$^{G85R}$ motoneurons whereas a counter-clockwise (Fig. 4D) was seen in 5 WT and 4 SOD1$^{G85R}$ motoneurons. Concerning the linear patterns of discharge (Fig. 4 B and C), they were obtained from 6 WT (3 with sustained firing) and 10 SOD1$^{G85R}$ motoneurons (2 with sustained firing). The different patterns of discharge were equally distributed in both WT and SOD1$^{G85R}$ motoneurons in our experimental conditions.

*Effect of Riluzole on the discharge pattern of SOD1 lumbar motoneurons*

In this set of experiments, we compared the effects of Riluzole on SOD1$^{G85R}$ (n=5) and SOD1$^{G93A}$ (n=2) motoneurons recorded in slices and submitted to two different stimulus protocols: a fast depolarizing constant current step (duration: 1s) inducing a continuous discharge of the motoneuron and a slow progressive depolarizing and repolarizing current (ramp protocol) lasting four seconds each way, allowing for spike frequency adaptation processes. This procedure was used to study the response of SOD1$^{G85R}$ (Fig 5) and SOD1$^{G93A}$ / Hb9-eGFP (Fig 6) motoneurons during bath application of Riluzole.

At low doses (5µM, Fig 5), Riluzole induced a reversible reduction of the adapted discharge frequency induced by the depolarizing step (Fig. 5, A2 and C). The ramp protocol (Fig. 5, D1-D3) showed a progressive inactivation of spiking, starting with the maximum current values, extending progressively to the repolarization phase until a complete blockade was obtained 30 minutes after the start of the perfusion. At this stage, the membrane potential time-course was not ohmic and displayed a rounded shape probably due to an unaffected underlying membrane current. After

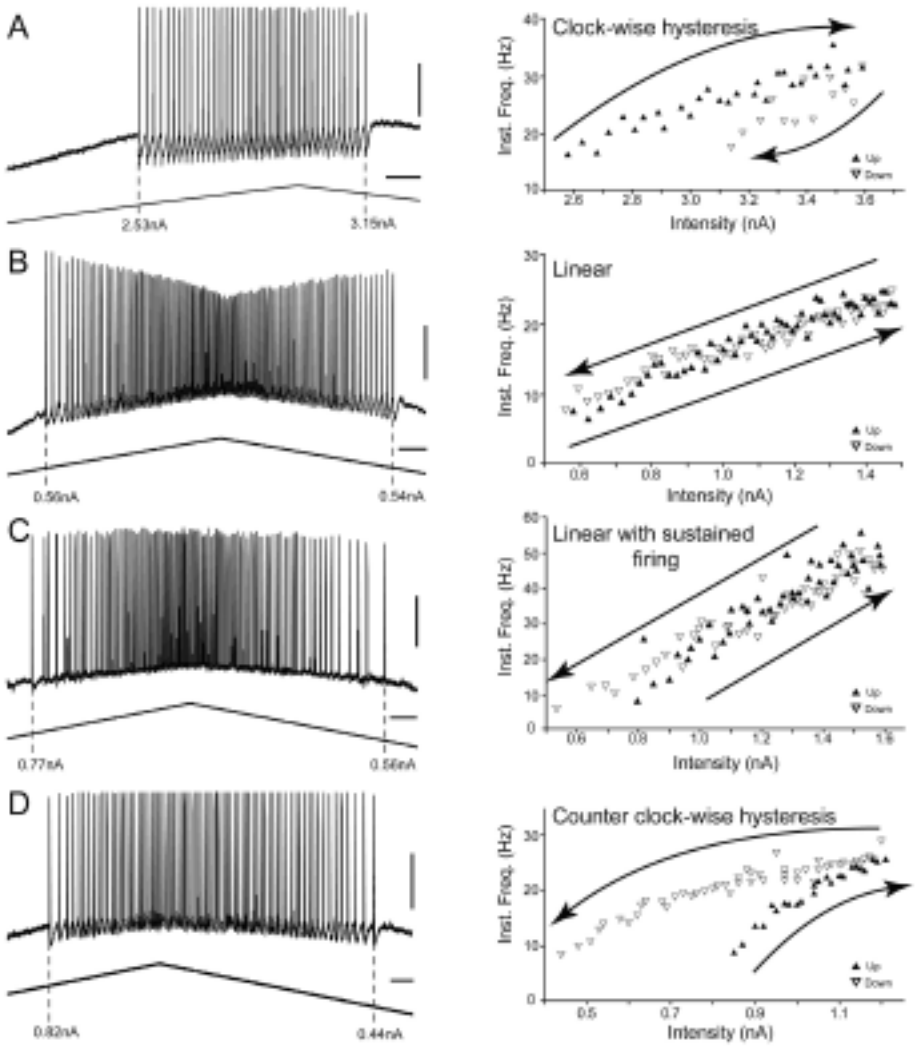


Fig. 4. - *Four patterns of discharge were recorded in response to current ramp stimulation both for WT and SOD1$^{G85R}$ motoneurons.*
A-D: Responses of 4 motoneurons (top traces) to a ramp current injections (bottom traces). Currents at spike recruitment and derecruitment are given under the dotted-lines. Graphs on the right part are plots of the instantaneous firing frequency as a function of the intensity of the injected current.
A: Clock-wise hysteresis pattern recorded from a P9 motoneuron; note the firing rate adaptation on the descending phase. Scale bars, 250ms and 20mV. Ramp duration 8.1 s, maximal intensity of injected current 3.6 nA.
B: Linear F-I relationship recorded from a P7 motoneuron; note the firing frequency curves that overlap on the ascending and descending phases. Scale bars, 500ms and 20mV. Ramp duration 10.8 s, maximal intensity of injected current 1.5 nA.
C: Linear F-I relationship with sustained firing on the descending part recorded from a P5 motoneuron. Scale bars, 250ms and 20mV. Ramp duration 5.4 s, maximal intensity of injected current 1.45 nA.
D: Counter clock-wise hysteresis pattern recorded from a P9 motoneuron. Note the acceleration of firing frequency on the descending part compared to the ascending one. Scale bars, 250ms and 20mV. Ramp duration 8.1 s, maximal intensity of injected current 1.15 nA.

washing, instantaneous firing frequency returned to control values but the motoneuronal response to the same current pulse started and terminated earlier even after 1 h washout (Fig. 5, D3).

Similar results were observed on WT (n=7) and SOD1$^{G93A}$ / Hb9-eGFP (n=2). As shown on fig 6C, the motoneurons in the lateral part of the ventral horn can be unambiguously identified by the presence of green fluorescent protein (GFP). Applying larger doses of Riluzole (10 µM) resulted in a fast (less than 3 minutes) and complete blockade of both the pulse (Fig. 6A) and the ramp (Fig. 6D) responses. In the case of the ramp response, the membrane potential time course after spike blockade was strictly ohmic (Fig. 6, D2), indicating a complete blockade of depolarizing (inward) membrane currents. Returning to standard perfusion medium induced partial recovery of the continuous discharge. The instantaneous firing frequency remained much lower than control values during both pulse and ramp stimulations. Furthermore, the

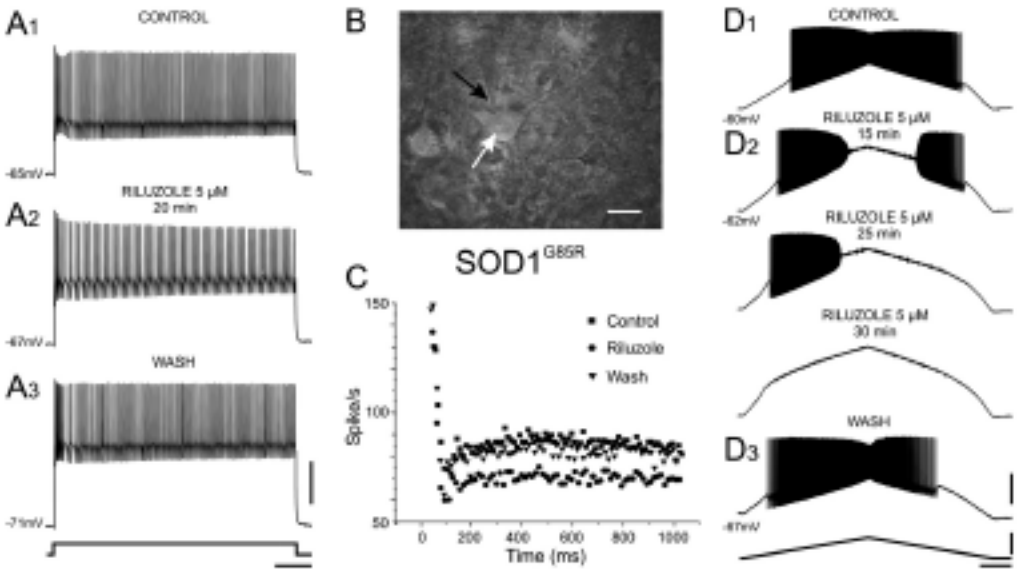


Fig. 5. - *Effects of Riluzole on the repetitive discharge of a SOD1$^{G85R}$ motoneuron.*
A1-A3: Repetitive firing of a SOD1$^{G85R}$ motoneuron (P8) in response to a pulse of current (2.5nA - 1s, bottom trace), before (A1), during (A2) and after (A3) the application of Riluzole (5 µM). Scale bars, 150ms and 30mV.
B: DIC infrared red photomicrograph of the recorded motoneuron (40x). The patch electrode (black arrow) was placed in contact to the soma of the motoneuron (white arrow).
C: Analysis of the instantaneous spike discharge frequency during the pulse of current illustrated in A. The instantaneous frequency of discharge was plotted as a function of time. Note that Riluzole application lowers the spike frequency revealing the implication of persistant $Na^+$ conductances in the repetitive firing.
D1-D3: Effect of Riluzole (same application than in A) on the motoneuron submitted to current ramp protocol. Note that the blockade of spiking was progressive and thorough. The fact that spiking was completely abolished suggests that Riluzole has also affected the $Na^+$ voltage sensitive channels. Scale bars, 1s, 4nA and 30mV.

discharge, which was symetrical on control recordings, became assymetrical with sustained firing during the repolarizing phase (Fig, 6, C and D3).

## DISCUSSION

The passive and active electrical properties of motoneurons from SOD1$^{G85R}$ mice were previously compared to those of wild type animals (3, 11). On the basis of electrical data on input resistance and membrane time constant measurements, we hypothesized that motoneurons from transgenic animals should be larger than that of WT, at the beginning of the second postnatal week (3). In the present work we found that the soma size, number and mean diameter of primary dendrites was comparable in both samples of motoneurons (n=9 for WT and n=8 for SOD1$^{G85R}$). However, the full 3D reconstructions of two motoneurons in each sample at postnatal ages P8-9

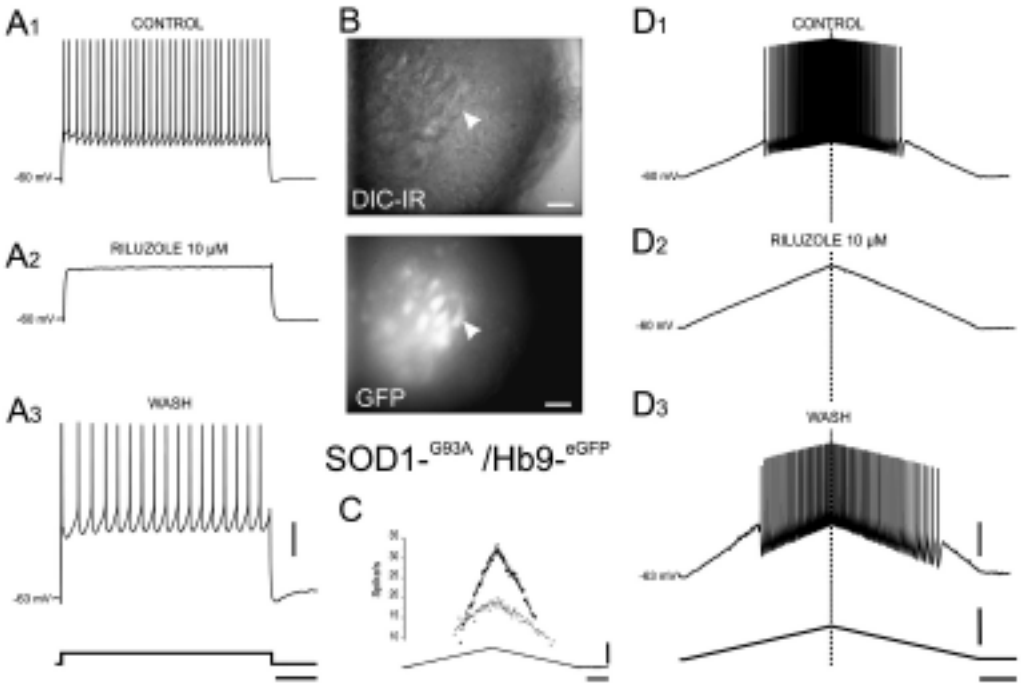


Fig. 6. - *Effects of Riluzole on the repetitive discharge of a SOD1$^{G93A}$/Hb9-$^{eGFP}$ motoneuron.*
A1-A3: Repetitive firing of the motoneuron in response to a pulse of current (1nA- 1sec, bottom trace), before (A1), after 3 minutes of perfusion of Riluzole 10 µM (A2) and after returning to standard perfusion (A3). Note the quick and complete blockade of discharge by Riluzole in A2. Calibration bars: 20 mV; 200 ms.
B: Photomicrographs of the recorded motoneuron (40x) with DIC infrared optics (upper) and with GFP fluorescence (lower). The recorded motoneuron is indicated with an arrowhead. Calibration bars: 50 µm.
C: Graphs of the instantaneous spike frequencies plotted as a function of time corresponding to the responses illustrated in D1 and D3. Same ramp as in D (1 nA; 1 s).

showed that dendritic trees in motoneurons from SOD1$^{G85R}$ mice had more branching nodes and terminals. They were also larger in terms of dendritic length and membrane surface area confirming the previous hypothesis. Whether these morphological alterations are due to a delayed maturation of supraspinal descending pathways or to a peripheral perturbation at the neuromuscular junction have yet to be determined. Whatever their origin, such morphological modifications like the higher number of branching nodes in the dendrites may have important functional implications for the motoneuron electrical behaviour (4, 15, 16).

Concerning the electrophysiological recordings, our results show that developing lumbar motoneurons from both WT and SOD1$^{G85R}$ mice displayed the four types of frequency vs intensity (F-I) relationships, as described in adult animals (2, 8). Furthermore, two types of discharge among them (counter clockwise and linear with sustained firing) suggest the presence of persistent inward currents (2, 8). The gain of motoneurons from SOD1$^{G85R}$ mice was affected in this postnatal period (3). Since activation of persistent inward currents modulate the slope of the (F-I) relationship (13, 19) and that the sodium persistent inward current has been involved in the toxicity of motoneurons in ALS models (18), we compared the effects of Riluzole on the discharge properties of WT, SOD1$^{G85R}$ and SOD1$^{G93A}$ motoneurons. No differences were seen with Riluzole during this postnatal period between the different groups of motoneurons in our experimental conditions. The blocking effect of Riluzole on the discharge of motoneurons was similar to that already described (22). We are now investigating whether the persistent inward calcium currents through the L-type calcium channels may be involved in the lower gain of motoneurons in SOD1 mouse pups. The present results confirm previous studies (1, 3, 11) that the maturation of lumbar motoneurons is altered by the SOD1 mutations linked to ALS.

## SUMMARY

Antidromically identified lumbar motoneurons intracellularly recorded in the entire brainstem/spinal cord preparation isolated from SOD1$^{G85R}$ postnatal mice (P3-P10) were labelled with neurobiotin and fully reconstructed in 3D from serial sections in order to analyse their morphology. This staining procedure revealed differences between WT and SOD1$^{G85R}$ dendritic trees for most metric and topologic parameters analyzed. A highly complex morphology of SOD1$^{G85R}$ motoneurons dendrites (increased number of branching points and terminations) was found and the dendritic trees were longer compared to the WT motoneurons. These morphological changes observed in P8-P9 motoneurons mice occurred concomitantly with a decrease in the input resistance and gain. During electrophysiological recordings, four patterns of discharge were observed in response to ramp stimulations, that were equally distributed in WT and SOD1$^{G85R}$ motoneurons. In slice preparation, whole cell patch-clamp recordings made from developing motoneurons in SOD1$^{G85R}$ and double transgenic SOD1$^{G93A}$/Hb9-eGFP mice showed that Riluzole, a blocker of per-

sistent inward sodium conductance, altered the repetitive firing in a similar way for the 2 strains.

These results show that the SOD1 mutations linked to familial ALS alter the development of the electrical and morphological properties of lumbar motoneurons.

*Acknowledgements.* - This research was supported by CNRS and a grant from The Association Française contre les Myopathies (AFM). J. A. received a doctoral fellowship from AFM. We thank Dr Brigitte Pettmann for the gift of double-transgenic SOD1-G93A/Hb9-eGFP mice and Dr Wilfrid Casseron for genotyping.

## REFERENCES

1. AMENDOLA, J., VERRIER, B., ROUBERTOUX, P., and DURAND, J. Altered sensorimotor development in a transgenic mouse model of amyotrophic lateral sclerosis. *Eur. J. Neurosci.*, **20**: 2822-2826, 2004.
2. BENNETT, D.J., LI, Y., SIU, M. Plateau potentials in sacrocaudal motoneurons of chronic spinal rats, recorded in vitro. *J. Neurophysiol.*, **86**: 1955-71, 2001.
3. BORIES, C., AMENDOLA, J., LAMOTTE D'INCAMPS, B., and DURAND, J. Early electrophysiological abnormalities in lumbar motoneurons in a transgenic mouse model of amyotrophic lateral sclerosis *Europ. J. Neurosci.*, In press., 2006.
4. BRAS, H., GOGAN, P., and TYC-DUMONT, S. The dendrites of single brain-stem motoneurons intracellularly labelled with horseradish peroxidase in the cat. Morphological and electrical differences. *Neuroscience*, **22**: 947-70, 1987.
5. BRUIJN, L.I., BECHER, M.W., LEE, M.K., ANDERSON, K.L., JENKINS, N.A., COPELAND, N.G., SISODIA, S.S., ROTHSTEIN, J.D., BORCHELT, D.R., PRICE, D.L. and CLEVELAND, D.W. ALS-linked SOD1 mutant G85R mediates damage to astrocytes and promotes rapidly progressive disease with SOD1-containing inclusions. *Neuron*, **18**: 327-338, 1997.
6. BRUIJN, L.I., HOUSEWEART, M.K., KATO, S., ANDERSON, K.L., ANDERSON, S.D., OHAMA, E., REAUME, A.G., SCOTT, R.W. AND CLEVELAND, D.W. Aggregation and motor neuron toxicity of an ALS-linked SOD1 mutant independent from wild type SOD1. *Science*, **281**: 1851-1854, 1998.
7. BRUIJN, L.I., MILLER, T.M. and CLEVELAND, D.W. Unraveling the mechanisms involved in motor neuron degeneration in ALS. *Annu. Rev. Neurosci.*, **27**: 723-749, 2004.
8. BUTTON, D.C., GARDINER, K., MARQUESTE, T., GARDINER, P.F. Frequency-current relationships of rat hindlimb alpha-motoneurones. *J Physiol., Lond.,* **573**: 663-77, 2006.
9. CLEVELAND, D.W. and ROTHSTEIN, J.D. From Charcot to Lou Gehrig: deciphering selective motor neuron death in ALS. *Nat. Rev. Neurosci.*, **2**: 806-819, 2001.
10. DAL CANTO, M.C., and GURNEY, M.E. A low expressor line of transgenic mice carrying a mutant human Cu,Zn superoxide dismutase (SOD1) gene develops pathological changes that most closely resemble those in human amyotrophic lateral sclerosis. *Acta Neuropathol. (Berl),* **93**: 537-50, 1997.
11. DURAND, J., AMENDOLA, J., BORIES, C. and LAMOTTE D'INCAMPS, B. Early abnormalities in transgenic mouse models of amyotrophic lateral sclerosis. *J. Physiol., Paris*, **99**: 211-220, 2006.
12. GURNEY, M.E., PU, H., CHIU, A.Y., DAL CANTO, M.C., POLCHOW, C.Y., ALEXANDER, D.D., CALIENDO, J., HENTATI, A., KWON, Y.W., DENG, H.X. *et al.* Motor neuron degeneration in mice that express a human Cu, Zn superoxide dismutase mutation. *Science*, **264**: 1772-5, 1994.

13. HOUNSGAARD, J, and MINTZ, I. Calcium conductance and firing properties of spinal motoneurones in the turtle. *J. Physiol.*, *Lond.,* **398**: 591-603, 1988.
14. JESSELL, T.M. Neuronal specification in the spinal cord: inductive signals and transcriptional codes. *Nat. Rev. Genet.*, **1**(1): 20-9, 2000.
15. KOROGOD, S.M., KULAGINA, I.B., HORCHOLLE-BOSSAVIT, G., GOGAN, P., TYC-DUMONT, S. Activity-dependent reconfiguration of the effective dendritic field of motoneurons. *J. Comp. Neurol*., **422**: 18-34, 2000.
16. KOROGOD, S.M., KULAGINA, I.B., KUKUSHKA, V.I., GOGAN, P. and TYC-DUMONT, S. Spatial reconfiguration of charge transfer effectiveness in active bistable dendritic arborizations. *Eur. J. Neurosci*., **16**: 2260-70, 2002.
17. KUO, J.J., SCHONEWILLE, M., SIDDIQUE, T., SCHULTS, A.N., FU, R., BAR, P.R., ANELLI, R., HECKMAN, C.J. and KROESE, A.B. Hyperexcitability of cultured spinal motoneurons from presymptomatic ALS mice. *J. Neurophysiol.*, **91**: 571-5, 2004.
18. KUO, J.J., SIDDIQUE, T., FU, R., and HECKMAN, C.J. Increased persistent Na(+) current and its effect on excitability in motoneurones cultured from mutant SOD1 mice. *J. Physiol.*, *Lond.,* **563**: 843-54, 2005.
19. LI, Y., BENNETT, D.J. Persistent sodium and calcium currents cause plateau potentials in motoneurons of chronic spinal rats. *J. Neurophysiol.*, **90**(2): 857-69, 2003.
20. LI, Y., BREWER, D., BURKE, R.E., ASCOLI, G.A., Developmental changes in spinal motoneuron dendrites in neonatal mice. *J. Comp. Neurol*. **483**(3): 304-17, 2005.
21. MCHANWELL, S., and BISCOE, T.J., The localization of motoneurons supplying the hindlimb muscles of the mouse. *Philos. Trans. R. Soc. Lond. B. Biol. Sci*., **293**: 477-508, 1981.
22. MILES, G.B., DAI, Y., and BROWSTONE, R.M. Mechanisms underlying the early phase of spike frequency adaptation in mouse spinal motoneurones. *J. Physiol. Lond.,* **566**:519-32, 2005.
23. PIERI, M., ALBO, F., GAETTI, C., SPALLONI, A., BENGTSON, C.P., LONGONE, P., CAVALCANTI, S. and ZONA, C. Altered excitability of motor neurons in a transgenic mouse model of familial amyotrophic lateral sclerosis. *Neurosci. Lett*., **351:** 153-56, 2003.
24. PUN, S., SANTOS, A.F., SAXENA, S., XU, L., and CARONI, P. Selective vulnerability and pruning of phasic motoneuron axons in motoneuron disease alleviated by CNTF. *Nat Neurosci.* **9**, 408-19, 2006.
25. ROSEN, D.R., SIDDIQUE, T., PATTERSON, D., FIGLEWICZ, D.A., SAPP, P., HENTATI, A., DONALDSON, D., GOTO, J., O'REGAN, J.P., DENG, H.X. *et al*. Mutations in Cu/Zn superoxide dismutase gene are associated with familial amyotrophic lateral sclerosis. *Nature*, **362**: 59-62, 1993.
26. URBANI, A., and BELLUZZI, O. Riluzole inhibits the persistent sodium current in mammalian CNS neurons. *Eur. J. Neurosci*., **12**: 3567-74, 2000.
27. WILLIAMSON, T.L., and CLEVELAND, D.W. Slowing of axonal transport is a very early event in the toxicity of ALS-linked SOD1 mutants to motor neurons. *Nat. Neurosci*., **2**: 50-6, 1999.